Sea surface temperature patterns in the Tropical Atlantic: Principal component analysis and nonlinear principal component analysis

Christian Sadem Kenfack, François Kamga Mkankam, Gaël Alory, Yves Du Penhoat, Mahouton Norbert Hounkonnou, Derbetini Appolinaire A Vondou, Gerard Bawe Nfor

Accepted Manuscript Online: 8 September 2016	Terr. Atmos. Ocean. Sci.	doi: 10.3319/TAO.2016.08.29.01

Accepted Manuscript

Sea surface temperature patterns in the Tropical Atlantic: principal component analysis and nonlinear principal component analysis

S. C. Kenfack[1, 2, 3, *], K. F. Mkankam [2], G. Alory [4], Y. du Penhoat [5], N. M. Hounkonnou[1], D. A. Vondou [2], and G. B. Nfor [3]

[1] International Chair in Mathematical Physics and Applications, Univ. of Abomey-Calavi, Cotonou, Benin

[2] Laboratory for Environmental Modelling and Atmospheric Physics, Department of Physics, University of Yaounde 1, Cameroon

[3] Mesoscopic and Multilayer Structures Laboratory (MMSL), Faculty of Science, Department of Physics, University of Dschang, Cameroon

[4] Laboratoire d'études en Géophysique et Océanographie Spatiales (LEGOS), Toulouse, France

[5] IRD; LEGOS, 14 Av. Edouard Belin, F-31400 Toulouse, France

Received 5 March 2016, revised 18 August 2016, accepted 29 August 2016

DOI: 10.3319/TAO.2016.08.29.01

*Corresponding author: kevinsadem@yahoo.fr

Sea surface temperature patterns in the Tropical Atlantic: principal component analysis and nonlinear principal component analysis

S. C. Kenfack · K. F. Mkankam · G. Alory · Y. du Penhoat · N.M. Hounkonnou · D.A. Vondou · G.B. Nfor

Key points of this manuscript

1. Results from PCA and NLPCA on SST of Tropical Atlantic Ocean were compared.
2. Ability of NLPCA to detect phenomena in the Tropical Atlantic Ocean was observed.

S. C. Kenfack

International Chair in Mathematical Physics and Applications, Univ. of Abomey-Calavi, Cotonou, Benin.

Laboratory for Environmental Modelling and Atmospheric Physics, Department of Physics, University of Yaounde 1, Cameroon

Mesoscopic and Multilayer Structures Laboratory (MMSL), Faculty of Science, Department of Physics, University of Dschang, Cameroon

Tel.: +237-78-005900

E-mail: kevinsadem@yahoo.fr

K. F. Mkankam

Laboratory for Environmental Modelling and Atmospheric Physics, Department of Physics, University of Yaounde 1, Cameroon

G. Alory

Laboratoire d''etudes en G´eophysique et Oc´eanographie Spatiales (LEGOS), Toulouse, France.

Y. du Penhoat

IRD; LEGOS, 14 Av. Edouard Belin, F-31400 Toulouse, France.

N.M. Hounkonnou

International Chair in Mathematical Physics and Applications, Univ. of Abomey-Calavi, Cotonou, Benin.

D.A. Vondou

Laboratory for Environmental Modelling and Atmospheric Physics, Department of Physics, University of Yaounde 1, Cameroon

G.B. Nfor

Mesoscopic and Multilayer Structures Laboratory (MMSL), Faculty of Science, Department of Physics, University of Dschang, Cameroon.

Abstract

The tropical Atlantic Ocean exhibits several modes of interannual variability such as the equatorial (or Atlantic Niño) mode, and meridional (or Atlantic dipole) mode. Nonlinear principal component analysis (NLPCA) is applied on detrended monthly Sea Surface Temperature Anomaly (SSTA) data from the tropical Atlantic Ocean (30°W-20°E, 26°S-22° N) for the period 1950 to 2005. The objective is to compare the modes extracted through this statistical analysis to those previously extracted through the more simple principal component analysis (PCA). It is shown that the first mode of NLPCA explains 38% of the total variance of SST compared to 36% by the first PCA while the second mode of NLPCA explains 22% of the total variance of SST compared to 16% by the second PCA. The first two NLPCA modes explain marginally more of the total data variance than the first two PCA modes. Our analysis confirms results from previous studies and, in addition, shows that the Atlantic El Niño structure is spatially more stable than the Atlantic dipole structure.

Keywords: PCA · NLPCA · SST · Tropical Ocean

Introduction

Thorough knowledge of our planet and its climatic variations increasingly becomes a major concern for humanity. Data collection techniques have witnessed significant progress over the past decades, especially with the use of satellites for the collection of global data. Given that the density of data increases over time, researchers have to work with more and more voluminous data whose analysis requires dedicated tools.

Sophisticated techniques such as principal component analysis (PCA) have become indispensable in extracting essential information from voluminous data sets (Von Storch and Zwiers, 1999). The weakness of this conventional method is that only linear structures can be extracted from data. This limitation means that nonlinear structures are either missed or misinterpreted by these methods. Since the 1980s, models of neural networks have been developed and Kramer (1991) used them to extend PCA abilities to the extraction of nonlinear relationships in a dataset, which defines the nonlinear principal component analysis

(NLPCA). The introduction of these two techniques has been determinant in the advancement of environmental science.

NLPCA can be performed by a variety of methods, e.g. the neural network (NN) model using multi-layer perceptrons (MLP) (Hsieh, 2004, 2007, Kramer, 1991) or the kernel PCA model (Scholkopf et al., 1998). NLPCA belongs to the class of nonlinear dimensionality reduction techniques, which includes principal curves (Hastie et al., 1989), locally linear embedding (LLE; (Roweis et al., 2000)) and isomap (Tenenbaum et al., 2000). The latter is the more complex technique, it finds a nonlinear transformation that preserves geodesics distances between data points (Aho et al., 1983). Several extensions have since been developed to help with treating the largest datasets (Bachmann et al., 2006, De Silva et al., 2004). Here, we focus on NLPCA based on neural network (Hecht, 1995, Malthouse, 1998). It has been successfully applied in the fields of atmospheric and oceanographic sciences (Hsieh, 2004, Monahan et al., 2003).

The tropical Atlantic Ocean is characterised by a strong seasonal cycle (Li and Philander, 1997, Xie and Carton, 2004), particularly in the Gulf of Guinea (GoG). Here, a zone of relatively cold sea surface temperature (SST) appears from June to September along and slightly south-east of the equator: the Atlantic Cold Tongue (ACT). This is the primary seasonal signal of SST in the equatorial Atlantic Ocean (Merle et al., 1980, Xie and Carton, 2004, Wauthy, 1983). This Atlantic signal appears almost all years in the East Equatorial Atlantic (EEA) and positions itself south of the Equator with a longitudinal extent to almost 20°W, centered and located a few degrees south of the Equator in the eastern part of the basin and slightly shifted equatorward (Caniaux et al., 2011). However, the detailed processes responsible for its variability are still the subject of considerable debate (e.g. Jouanno et al., 2011a, b)).

The Atlantic Ocean has a strong impact on the West African climate, especially on precipitation. In particular, the ACT strongly affects the West African Monsoon (WAM) (Okumura and Xie, 2004, Thorncroft et al., 2011). Its seasonal appearance intensifies the southerly winds in the GoG, which pushes a zonal rainband from the northern coast of the GoG to the sahelian region farther inland. It strengthens the north-south land-sea temperature contrast, enhancing the monsoonal flow that leads to a further decrease in SST. Due to the effect of the ACT on the WAM that suggests potential rainfall predictability, the problem of understanding the inter-relationship between the ACT and the WAM remains at the center of many research endeavours (Hagos and Cook, 2008, Leonard and Matthew, 2014, Okumura and Xie, 2004). Caniaux et al. (2011) shows that there is

interannual variability in the ACT spatial pattern in GoG, which is not fully understood. Picaut et al. (1984) did a comparison between seasonal and interannual variability of SST in the tropical Atlantic. The result is that interannual changes in SST are largest in regions where the seasonal SST signal is large, including the ACT region, which suggests that the tropical Atlantic interannual variability is strongly linked to the seasonal cycle. However, while seasonal SST fluctuations are large, interannual variations in the Atlantic are modest in amplitude (Li and Philander, 1997). Within the last decades, two primary modes of interannual variability have been identified in the tropical Atlantic (e.g. Servain and Merle, 1993, Xie et al., 1999)): the equatorial and meridional modes.

The equatorial mode is responsible for SST variability in the GoG mainly, and is identified by abnormal changes in the equatorial thermocline slope resulting from zonal-wind anomalies in the western tropical Atlantic. This mode coincides with the seasonal development of the equatorial cold tongue.

When the trade winds intensify in the western Atlantic, the equatorial thermocline slope increases and negative SST anomalies develop in the GoG, reinforcing the ACT; conversely, when trade winds weaken, the equatorial thermocline slope decreases and positive SST anomalies develop in the GoG (Servain and Amault, 1995). Indeed, a shallow thermocline in the GoG means that cool subsurface water is able to upwell to the surface and to create cold SST anomalies. This type of mechanism is found in Moore et al. (1978), Picaut (1983), and Katz (1997) and the relevant theory in Zebiak (1993) and Servain and Amault (1995).

Many studies emphasize the similarity between the El Niño Southern Oscillation (ENSO) in the Pacific Ocean and this equatorial Atlantic mode, therefore also called Atlantic Niño (Delecluse et al., 1994, Horel et al., 1986, Xie and Carton, 2004). However, the Atlantic Niño is much weaker than its Pacific counterpart (Carton and Huang, 1994, Latif and Grötzner, 2000, Servain et al., 2003, Zebiak, 1993). A relationship between the Atlantic Niño and Pacific variability has also been suggested by some studies (Carton and Huang, 1994, Servain and Merle, 1993). The meridional mode is characterized by a north- south inter-hemispheric gradient of SST anomaly that has no equivalent in the Pacific Ocean (Servain et al., 1999). It is most pronounced during the equatorial warm season from March to May (Clara et al., 2010). Xie and Tanimoto (1998) demonstrated how wind forcing induces this mode. Many observational (Enfield et al., 1997) and modeling (Huang et al., 2002) studies have shown that the ENSO influence on the tropical Atlantic is strongest in the North Tropical Atlantic, with Atlantic warming occurring 4-5 months after the mature phases of Pacific warm events (Xie and Carton, 2004). In particular, this means that the meridional mode, is

significantly influenced by ENSO (Czaja et al., 2002). A link between the equatorial mode and the meridional mode has also been suggested by Servain et al. (1999). A recent study (Richter et al., 2012) distinguishes two types of Atlantic Niño referred as canonical Atlantic Niño and non-canonical Atlantic Niño. While the canonical event follows the conventional ENSO mechanism, the non-canonical event involves southward temperature advection from the northern tropical Atlantic. This process could connect the meridional to the equatorial mode. Alternatively, the connection could involve a transmission of thermocline depth anomalies through equatorial waves (Foltz and McPhaden, 2010). At longer time scales, an observational study (Tokinaga et al., 2011) revealed robust changes in the equatorial Atlantic over the past six decades, most notably a locally enhanced SST warming in the GoG and a weakening of the ACT variability. Additional studies are necessary for understanding long term variations in the tropical Atlantic, especially in ACT, equatorial and meridional modes.

The NLPCA technique has already proved useful in a climatic context. It has been applied on SST to study climate variations in the tropical Pacific (e.g. Hsieh, 2001, Li et al., 2005). In particular, it has shown that the spatial variability associated with the ENSO phenomenon is non-linear (Hsieh, 2004, 2007). The subsurface thermal structure of the Pacific Ocean was also studied using the NLPCA (Tang and Hsieh, 2003). Moreover, this method has been used for some atmospheric studies of sea level pressure and air temperature over Canada (Monahan, 2001). Also, in the South China Sea, Chen et al. (2010) applied NLPCA on SST and showed that this statistical method accounts for more variance of the total variables in comparison with linear PCA and brings a finer analysis of interannual variability. While PCA has been frequently used in the above studies of tropical Atlantic variability, NLPCA has never been applied in this region, to our knowledge. The internannual modulation of the ACT, which strongly affect African climate, might better be understood using the NLPCA.

The aim of this work is to exhibit the main patterns of the variability of SST in the tropical Atlantic Ocean using NLPCA. This paper is an attempt, using an advanced method of PCA, to evaluate and describe the main modes of tropical Atlantic Ocean. We apply PCA and NLPCA on data from the tropical Atlantic SST. The paper is organized as follows: Section 2 is a brief description of the PCA, NLPCA methods and SST data we use. The third part describes the results of these methods on the Atlantic SST. The last part concludes.

2 Method and data

Linear methods of dimensionality reduction like PCA are useful tools for handling and interpreting high dimensional data. On the other hand, several nonlinear dimensionality reduction methods such as kernel PCA (kPCA), Isomap, local linear embedding (LLE) and NLPCA have been developed. Many of these nonlinear methods, including most of the differential geometry based methods and some of the neural network based methods, were originally developed in machine learning and machine vision communities for the purpose of extracting low-dimensional information from data sets applications; such as object identification and feature tracking. Both Isomap and NLPCA emanate from the PCA. Isomap is a geometrical/statistical method identified with (objective 1) cited in section 2.1 while NLPCA (discussed later) is a Neural network method identified with (objective 2) in the same paragraph. Isomap is the most straight way to use the geodesic distance for nonlinear projection. The goal of the Isomap (Tenenbaum et al., 2000) is to preserve the geodesics rather than the Euclidian distances. It has been broadly used in a large series of signal and image processing, pattern recognition and data analysis applications (Gámez et al., 2004). To apply NLPCA, an initial dimensionality reduction step is required to reduce the dimensionality of the inputs so that a neural network of reasonable size can be used. Unlike some other nonlinear dimensionality reduction methods, NLPCA cannot be used directly with observed or modelled SST data sets. This contrasts with methods such as Isomap , where gridded data sets can be handled without preprocessing. The key factor that distinguishes Isomap from NLPCA is that Isomap uses a distance function that approximates geodesic distances in the data, while the latter employs Euclidean distances in the data space. In this work we focus our attention on PCA and NLPCA.

2.1 Principal component analysis

PCA is the method which analyzes the variability of a single field (Rainfall, SST, etc). Commonly, it is used for two objectives: (1) Reducing the number of variables comprising a dataset while retaining the variability in the data and (2) identifying hidden patterns in the

data, and classifying them with little loss of information (representing the variables by a small number of components). In other words to extract features or recognize patterns from the dataset. In this paper, it is the latter which attracts our attention. Mathematically, the aim of PCA (Fukuoka, 1951, Lorenz, 1956) is to achieve a decomposition of a continuous space-time field $Y(i,t)$, where i and t denote respectively spatial position and time, as

$$Y(i,t) = \sum_{k=1}^{l} \mathbf{a}_k(i) v_k(t) \qquad (1)$$

where k is the index which characterize the difference between modes and l is the number of modes contained in the field, using an optimal set of basic function of space $\mathbf{a}_k(i)$ and expansion function of time $v_k(t)$. It finds the spatial patterns of variability, their time variation, and gives a measure of particular structure of each v_k pattern. To present the concept, we suppose that we have a gridded data set composed of a space-time field $Y(i,t)$ in the form $\mathbf{x}$, such as SST, at time t and spatial position i. The observed field is then represented in the form:

$$\mathbf{x}(t) = \left[x_1, x_2, ..., x_l\right] \qquad (2)$$

where x_i is a time series containing s observations. PCA is based on the analysis of the covariance matrix e.g. (Hannachi et al., 2007), which the variances are diagonal elements of the matrix and the covariance values are off diagonal terms. By dividing the covariance matrix by the variances the correlation matrix will be obtained which is the covariance matrix of the normalized variables. The eigenvalues and eigenvectors of the covariance matrix are then computed. Unlike the original data vectors, the eigenvectors are uncorrelated and orthogonal. The projection of the original data vectors onto the eigenvectors space yields the principal components. In general, fewer eigenvectors are required to sufficiently represent the data. In practice the PCA technique aims at finding a new set of variables that capture most of the observed variance from the data through linear combinations of the original variables. All the components $\mathbf{a}_k$ and v_k must be determined and one of the method is to find those components successively from the first $(v_1, \mathbf{a}_1)$ to the last $(v_l, \mathbf{a}_l)$. Then PCA looks for v which is a linear combination of the x_i and an associated vector, with

$$v = \mathbf{a}.\mathbf{x}(t) \qquad (3)$$

so that $\left\langle \left\| \mathbf{x}(t) - \mathbf{a}v(t) \right\|^2 \right\rangle$ is minimized, and where $\langle ..... \rangle$ denotes a time mean.

In other words the goal is to find v_1 and $\mathbf{a}_1$ such that the last relation is minimized. v_1 is called the first principal component (PC), a time series, while $\mathbf{a}_1$ is the first eigenvector of the data covariance matrix, also called an empirical orthogonal function, (EOF), that describes a spatial pattern. From the residual, $\mathbf{x} - \mathbf{a}v$, subsequent modes can be calculated in the same fashion. These methods have been performed using NN and become nonlinear principal component analysis.

2.2 Nonlinear principal component analysis

The fundamental difference between NLPCA and PCA is that NLPCA allows a nonlinear mapping from $\mathbf{x}$ to v (denoted in this part by u to make difference between NLPCA and PCA terms) whereas PCA allows only a linear mapping. A large number of specialized neural networks and learning algorithms have been proposed to perform principal component analysis (PCA) such as Isomap and NLPCA. There is no conclusive study that shows which approach is superior. The essential problem with nonlinear methods such as Isomap is that there exist few theoretical results underpinning the numerical algorithms. The network model has greater flexibility than the hierarchical model for handling complex spatial relationships.

In Fig.1 the input column vector $\mathbf{x}$ of length l are mapped to the neurons in the hidden layer and the transfer function q_1 maps from $\mathbf{x}$ to the first hidden layer (the encoding layer), represented by $h^{(x)}$, a column vector of length m, with elements

$$h_k^{(x)} = q_1\left[\left(\mathbf{W}^{(x)}\mathbf{x} + \mathbf{b}^{(x)}\right)_k\right], \qquad (4)$$

$(k = 1, ..., m)$, with the sigmoid function

$$q_1 = \tanh$$

where $\mathbf{W}^{(x)}$ are weight matrices and $\mathbf{b}^{(x)}$ is bias parameter vector. The dimensions of x and $\boldsymbol{h}^{(x)}$ are l and m, respectively, where $\mathbf{x}$ is the input column vector of length l, and m is the number of hidden neurons in the encoding and decoding layers for u. The neurons u are calculated from a linear combination of the hidden neurons $\boldsymbol{h}^{(x)}$. A second transfer function q_2 maps the encoding layer to the bottleneck layer containing a single neuron, which represents the nonlinear principal component u, with

$$u = q_2\left[\boldsymbol{W}'^{(x)} \cdot \boldsymbol{h}^{(x)} + \overline{\mathbf{b}}^{(x)}\right] \quad (5)$$

with identity function q_2. These mappings are standard feed forward NNs and are capable of representing any continuous function mappings from $\mathbf{x}$ to u.

On the right side of Fig.1 the top NN (a standard feed forward NN) maps u to $\mathbf{x}'$ in two steps:

A transfer function q_3 maps from u to the final hidden layer (the decoding layer) $\boldsymbol{h}^{(u)}$,

$$h^{(u)} = q_3\left((\boldsymbol{W}'^{(u)}u + \mathbf{b}^{(u)})_k\right), \qquad (6)$$

with $q_3 = \tanh$ and $(k = 1,.....,m)$; followed by q_4 mapping from $\boldsymbol{h}^{(u)}$ to $\mathbf{x}'$, the output column vector of length l,with

$$x_i' = q_4\left((\boldsymbol{W}^{(u)}\boldsymbol{h}^{(u)} + \overline{b}^{(u)})_i\right) \quad (7)$$

with identity function q_4. To any given accuracy, provided large enough l and m are used to maximize by finding the optimal values of $\boldsymbol{W}^{(x)}$, $\boldsymbol{b}^{(x)}$, $\boldsymbol{W}'^{(x)}$ and $\overline{b}^{(x)}$.

The cost (Hsieh, 2001) function

$$J_1 = \left\langle \left\| \mathbf{x}' - \mathbf{x} \right\|^2 \right\rangle \quad (8)$$

is minimized by finding the optimal values of $\boldsymbol{W}^{(u)}$, $b^{(u)}$, $\boldsymbol{W}'^{(u)}$ and $\overline{b}^{(u)}$. The mean square error (MSE) between the output $\mathbf{x}'$ and the original data $\mathbf{x}$ is thus minimized. Without loss of generality, we impose the constraint $\langle u \rangle = 0$, hence

$$\overline{b}^{(x)} = -\left\langle \boldsymbol{W}'^{(x)} \cdot \boldsymbol{h}^{(x)} \right\rangle \quad (9)$$

The total number of free (weight and bias) parameters used by the NLPCA is then $2lm + 4m + l$. Furthermore, we adopt the normalization condition that $\langle u^2 \rangle = 1$. This condition is approximately satisfied by modifying the cost function to

$$J = \left\langle \left\| \mathbf{x} - \mathbf{x}' \right\|^2 \right\rangle + \left(\langle u^2 \rangle - 1\right)^2 \quad (10)$$

The choice of m, the number of hidden neurons in both the encoding and decoding layers, follows a general principle of parsimony. A larger m increases the nonlinear modeling capability of the network, but could also lead to overfitted solutions. If q_4 is the identity function, and $m = 1$, then Equation (9) implies that all $\mathbf{x}'$ are linearly related to a single hidden neuron, hence there can only be a linear relation between the $\mathbf{x}'$ variables. For nonlinear solutions, we need to look at u. In effect, the linear relation (3) is now generalized

to $u = f(\mathbf{x})$, where f can be any nonlinear function represented by a feed forward NN mapping from the input layer to the bottleneck layer; and instead of $\left\langle \left\| \mathbf{x}(t) - \mathbf{a} \cdot v(t) \right\|^2 \right\rangle$, $\left\langle \left\| \mathbf{x} - g(u) \right\|^2 \right\rangle$ is minimized, where g is the general nonlinear function mapping from the bottleneck to the output layer. The residual, $\mathbf{x} - g(u)$, can be input into the same network to extract the second NLPCA mode, and so on for the higher modes.

That the classical PCA is indeed a linear version of this NLPCA can be readily seen by replacing all the transfer functions with the identity function, thereby removing the nonlinear modeling capability of the NLPCA (Hsieh, 2001). Then the forward map to u involves only a linear combination of the original variables as in the PCA. A number of runs (mappings from u to $\mathbf{x}'$) used to find the solution with the smallest MSE. The NLPCA here generalizes easily to more than one hidden layer mappings, as two hidden layer mappings may outperform single hidden layer mappings in modeling complicated nonlinear functions. A reconstruction using a single PCA mode is a poor approximation to the input data and the greater freedom available to the NLPCA network allows it to produce a nonlinear fit which represent better the variability in the input data.

2.3 Data

We used monthly Atlantic sea surface temperature (SST) data, which is the reconstruction sea surface temperature (ERSST) data set (Smith et al., 2003) from the NOAA National Climatic Data Center. A climatologically annual cycle was calculated by averaging the data for each calendar month, and monthly SST anomalies (SSTAs) were defined relative to this annual cycle. This data set is a mixture of satellite and in situ data with a spatial resolution of 2° × 2° from 1950 to 2005. Because of the interest in the El Niño, dipole and cold tongue phenomenon in the Atlantic, an empirical orthogonal analysis was made of tropical Atlantic data between 26°S to 22°N and 30°W to 20°E. Thus there are (26 × 25) 650 spatial points, 215 points of missing SST data on the continent, and (26 × 25-215) 435 spatial and (56×12) time existing points. The SSTA have long-term trends. In order to minimize the effect of these trends on the analysis, we have eliminated the linear trends from datasets at each spatial location using the least squares technique. Thus, detrending the monthly anomaly, our primary dataset was formed.

3. Tropical Atlantic Sea surface temperature

Eigenvectors with the largest percentages are usually associated with physical processes. EOFs provide a series of eigenvectors, each of which contains a percentage of the temporal variability of the data. Figs. 2a and 2b show the first two modes of EOF and their corresponding principal components (PCs) (Figs. 3a and 3). The spatial patterns associated with two SST modes are shown in Fig.2 as homogeneous correlation maps EOF1 and EOF2. The two EOF modes together account for 52% of the total monthly SST variance. Individually, they explain 36% and 16% of the total variance of SST. The other components explain less than 14% of the total variance and will not be discussed further. The two modes differ in their spatial expressions. It should be noted that the sign of the EOF is arbitrary; however, the product of the EOF and the PC time series recovers the correct polarity of the mode in any given grid box and time. For SSTA data, we choose the nonlinear PCA model $m = 3$ and 3931 parameters which greatly exceeds the number of time points. There are still far too many spatial variables (number of points in the selected space) for this dataset to be directly analyzed by the NLPCA. To reduce the number of input variables, the SSTA data is pre-filtered by PCA. The NLPCA method used here is identical to that used by Hsieh (2004). Monahan (2001) used same for the study of El Niño/La Niña. The difference is that the former used 3 PCs or 3D-approximation while the latter used 10 PCs or 10D-approximation as inputs to the NLPCA, and the results are similar, which means that the principal characteristics of the phenomenon (El Niño/La Niña) are contained within the first 3 PCA modes. This implies that a certain minimum number of PCs can be sufficient to capture a phenomenon. In our case, to select the number of PCs, we used the Guttman-Kaiser criterion; where only the modes with eigen values greater than the average eigen value were retained (Jackson, 1991, Landman and Tennant, 2000). In this study this criterion gives 20 PCs whose total variance is 99%. It is true that less than 20 can still also give the expected results based on the rule of thumb (North et al., 1982). Then the first 20 PCs are used as the input to the NLPCA network. Each input variable is normalized by subtracting its mean and then dividing by the standard deviation of the first PC (Hsieh, 2001). Scatter plots of the 3 leading principal component time series are shown by the solid blue dots in Fig.4. All four projections are shown because it is difficult to understand the structure of the NLPCA approximation from a single projection. This is particularly evident in Fig.4c, where the curve, viewed edge-on, appears to be self-intersecting, whereas, in fact, the other projections demonstrate that this is not the case.

3.1 Atlantic Cold Tongue

EOF1 exhibits (Fig.2a) a high variance in coastal Angola, which extends from the coast to the west between 6°S and 2°N and EOF2 exhibits (Fig.2) large variances in two places: (1) at the Equator between 5°S and 2°N and (2) along the Gabon coast. EOF1 mode (Fig.2a) accounts for up to 36% of the total variance with the region of largest amplitude around the Angola coast. The signal decreases from East to West between 15°S and 2°N. The GoG is identified by abnormal changes in the equator and eastern part. The SSTA signature of the first mode is mainly confined to the eastern equatorial region. This first mode presents a structure for which the pattern is more closely confined to the eastern basin and spanning a range of latitudes (Zebiak, 1993) near the Angola coat. This spatial structure is characterized by a zonal pattern symmetric about the equator, with warm or cold SSTs appearing in the eastern equatorial basin to the south and north. The pattern of the first mode captures the zonal mode pattern in the tropical Atlantic (Carton and Huang, 1994, Handoh and Bigg, 2000, Huang and Shukla, 1997, Ruiz-Barradas et al., 2000, Zebiak, 1993). By multiplying EOF1 with its related PC, we observe some typical ACT cold years, such as 1990, 1992, 1997, 2005 and warm years 1984, 1987 and 1998 (Caniaux et al., 2011). At the end of 1964 and again in 1967, there was a general cooling over most of the Atlantic and particularly strong in the east. Likewise, in 1966 there is much less warming in these same areas. The year of 1969 is revealed as being warmer as reported in a previous study (Servain and Legler, 1986). This mode mainly presents interannual variability in the tropical Atlantic. In addition, the correlation coefficient between PC1 and Atlantic Niño SST index is 0.82. The Atlantic Niño SST index is defined as the area-averaged SSTA over 3°S-3°N, 20°W-0° (Zebiak, 1993). Hence, this picture resembles the equatorial mode. The first mode (Fig.4) of NLPCA explains 38.6% of the variance of the given EOFs, i.e 38% of the total variance of SSTA compared to 36% explained by the first PCA. The projection of NLPCA mode in the planes defined by pairing PC1, PC2, and PC3 are shown in red in Fig.4. The NLPCA mode 1 is slightly coincident with the projection onto PC1 indicated by the green line in the plots. Unlike the PCA, the NLPCA shows the nonlinear form in SSTA structure. The SSTA manifests itself as a *Wave*-shaped curve on the non linear graph of the first nonlinear mode between the minimum and maximum values of its principal component u. The non linearity of the sinuosity observed in Fig.4a is modest and the maximum of PC1 is less than the absolute value of the minimum of PC1. This insinuates that we have a very cold and very warm event

in the Atlantic region. It seems as if the two (ACT and Atlantic Niño) evolve together because their correlation coefficient is 0.94. Fig.5 is a plot of the normalized time series of nonlinear principal component (NLPC), which bears a strong resemblance to the ACT time series. This"ACT index" is obtained by computing the inter-annual mean of SSTA in the ACT zone (in the box from 5°S to 2°N and from the coast to 20°W during the ACT period (June-August) Caniaux et al. (2011)). Normalization is obtained by subtracting the mean and dividing by standard deviation. The correlation coefficient between the normalized ACT index, nonlinear principal component and linear principal component are respectively 0.85 and 0.8.

Fig.6 shows the reconstructed field of SST anomaly for some values of the first nonlinear component u. It is obtained by choosing a particular value of u associated with each of twenty PCs and multiplied by the associated EOFs. Eight values of u are chosen equitably from minimum to maximum. To display the sequences of ACT (which correspond to the value of u as Fig.4a indicates) and only the eight equitable interval (Fig.6) values of u are selected: −3.14,−0.98, −0.57, −0.25, 0.06, 0.31, 0.54, and 1.08. It observed that the spatial distribution varies with each selected value of u. This variation from the minimum (strong activity of Atlantic cold tongue) to maximum (low activity of Atlantic cold tongue) of the eight values of u shows a contrast between the north-east and southwest of 5°S. Those patterns are repeated from a to h. We note in Fig.6 that the cold year of ACT is more intense than the warm one and ACT distribution is quasi-linear in space. This result is confirmed by the high correlation coefficient between NLPCA mode 1 and PCA1. As afore mentioned, Figs.6a and 6h exhibit strong and weak ACT, respectively.

The differences in strong/weak ACT symmetry in Fig.6 can be compared with the results of composite analysis. The simplest approach is to compute the mean of NLPC. Warm and cold events are defined in each time series as events whose amplitudes are greater or less than the mean of NLPC; the warm and cold events have positive and negative signs, respectively. Thereafter, we compute the mean of each group; i.e. for the warm or cold years during the ACT period (JJA). This averaged period was used for the composites because JJA displays the period which the surface area at less than 25°C is greater than the empirical threshold surface area at 0.40×10^6 km^2 (Caniaux et al., 2011). The mean for the strong ACT is represented by Fig.7.a and for the weak by Fig.7.b. The largest SSTA is located in the eastern part during average weak ACT events and centered in the same region during average strong ACT events. We may observe that the pattern of these two types of ACT is quasi symmetric.

3.2 Atlantic Niño

Xie and Carton (2004) shows that Atlantic Niño is most pronounced in boreal summer coinciding with the seasonal development of the equatorial cold tongue. Fig.6a represents the coldest year and Fig.6h the year of the warmest ACT, which is not the warmest year but the year of weak ACT corresponding to Atlantic Niño. Then the weak ACT can be regarded as the conventional El Niño. Joke and Michael (2013) results show that the Atlantic Niño mode is more strongly damped than Pacific Niño. In this study, unlike in the Pacific Ocean where Hsieh (2004) shows that the Pacific El Niño is asymmetric, the spatial variability of this mode in the Atlantic Ocean is more linear than the El Niño/Southern Oscillation (ENSO). This is a new understanding between Atlantic Niño and Pacific Niño.

The results presented in Fig.6.e, f and g characterized the non canonical Atlantic Niño with negative anomalies in the northern tropical Atlantic and Fig.6h characterized the canonical Atlantic Niño with positive anomalies in the northern tropical Atlantic. The first NLPCA mode successfully passes through the canonical El Niño states, non-canonical El Niño states and ACT states as u varies continuously from its minimum value to its maximum value. Therefore, NLPCA is capable of simultaneously capturing many more pictures in the Atlantic Ocean. In addition, it gives a more accurate description of the El Niño states (Fig.6) than the first PCA mode (Fig.2a), which did not fully represent the canonical and non-canonical Atlantic Niño. With a linear approach, it is generally impossible to have simultaneous results.

3.3 Atlantic dipole

A north-south inter-hemispheric gradient of SST anomalies is observed in the second mode of PCA. The SSTAs show a remarkable meridional gradient, with significant positive anomalies spreading from the North African coast into the northwestern tropical Atlantic and significant negative anomalies in the south. There is, however, a local maximum in the tropics which has a sign, indicating that the two regions are quite strongly out of phase. PC2 and Atlantic dipole SST index are well correlated (Fig.3) with correlation coefficient of 0.66. Then EOF2 displays an opposite phase between the North and South parts of 6°S. This picture is consistent with the Atlantic dipole (Servain et al., 1999).

We now turn to NLPCA SST mode 2 results (Fig.8 and Fig.9), The NLPCA network architectures used for calculating NLPCA SST mode 2 are essentially the same as those of Hsieh (2001); three hidden layer neurons with all training and fitting parameters identical to

the configuration used for calculating NLPCA SST mode 1. The explained variance results show that the NLPCA mode 2 explains more variance as the second principal components. For the observational SST data, NLPCA SSTA mode 2 explains 22% of the total data variance, compared to 38% for NLPCA SST mode 1. The first two NLPCA modes between them explain marginally more of the total data variance than do the first two PCA modes.

We therefore expect that the nonlinearity will be more pronounced in the Figs.9 in the reconstruction plots for NLPCA mode 2. The reconstruction is obtained as we did in the case of NLPCA mode 1. We also display the sequences of Atlantic dipole and only the eight equal interval values of the second NLPC mode are selected: −2.71, −1.12, −0.80, −0.38, −0.059, −0.052, 0.37, and 0.70. This variation from the minimum (strong gradient) to maximum (weak gradient) of the eight values of the NLPC of the second NLPCA mode shows a contrast between the north-west and south-west. There is clear nonlinearity in the distribution from NLPCA SST mode 2. The main characteristic of the Atlantic dipole is captured, with the South Pole shifted towards the coast with different signs. The main pattern of variation between large negative and positive values of NLPCA mode 2 is a dipole; with each pole on either side of the equator with a different sign (Fig.8). This meridional mode (Fig.8) is exhibited in the second mode of NLPCA. Figs. 8b, 8c, 8d show the displacement of southern counterpart of the dipole, which confirms the asymmetry of the meridional mode. This shows that the variability of the second mode, which resembles the meridional mode one, can change from year to year. Regardless of Fig.8, there were interesting patterns that came out in the second NLPCA. There is some discrepancy between the Atlantic dipole structure. During the strong gradient (meridional gradient between the two lobes, Fig.8a) events the core of the southern lobe is centered around 15°W during the strong gradient and around 20°W during some weak events (Fig.8f). The Atlantic dipole in Fig.8a is similar to that in Fig.8f but the southern lobe is not located at the same place. The situation in the South lobe is unstable. We also observed that the south lobe is missing in Figs. 8b, c, d. This is not surpring because it is observed in some studies (Rajagopalane et al., 1998, Servain, 1991) that the Atlantic dipole exhibits decadal time scales. It is confirmed by Xie and Carton (2004) whose analysis showed that meridional dipole rarely occurs. Compared to Fig.8a, the southern lobe of Fig.8f is somewhat shifted to the east while the northern lobes have weaker anomaly. Fig.10 shows the time series of NLPC mode 2 and Atlantic dipole index with the correlation coefficient of 0.9. When observing the Atlantic dipole structure, we may realise that the sequential evolution of the phenomenon from Fig.8a to Fig.8h is interrupted, implying that the phenomena is not observed each year which is not also suprising as results. However, we

may observe that the south counterpart of the dipole has a displacement. Thus the spatial variation of the meridional mode changes meaning that the phenomenon cannot happen in the same place every year.

4. Discussion

There are many possible schemes for rotation of PCA (RPCA); the varimax (Kaiser, 1958) being the most popular. Both RPCA and NLPCA take the PCs from PCA as inputs. There is an important difference between PCA and rotated PCA methods; as it is generally impossible to have a simultaneous solution: explaining maximum global variance of the data and approaching pattern recognition. NLPCA can give both information, thus the nonlinearity in NLPCA unifies the PCA and rotated PCA approaches (Hsieh, 2001). In this paper, in terms of variance, the first rotated PCA explained 31% of the total variance (not shown), versus 36% by the first PCA mode. The first PCA exhibits a more accurate description of the ACT than the first RPCA mode. The combination of all two SST EOFs yields the major events in the tropical Atlantic. In this section it is known from SSTA that PCA points out the interannual principal mode in the Atlantic Ocean. NLPCA can give more information about this variability.

It is observed that the NLPCA mode 1 better represents the inter-annual variability of ACT than linear PCA mode 1. Fig.6b corresponding to 0.75 min(u) is similar to EOF1. So, NLPCA explains variances extracted by PCA and gives more information, which is not obvious by analysis with the PCA. Linear PCA method describes the evolution in time of a standing oscillation with fixed spatial structure and time varying amplitude. NLPCA is not so constrained, and therefore its power lies in characterizing more complex lower-dimensional structures (Monahan, 2001). The analysis of the two curves of (Fig.5) indicates that NLPCA can give more information about ACT. SSTA is stronger in ACT than other parts of Atlantic Ocean except in the Angola coast where it is strongest. This view appears to corroborate to the observations of Hirst and Hantenrath (1983) and of Rouault et al. (2003) that the variability in tropical southeast Atlantic SST is strongest in the Angola Benguela frontal current zone region near 15°S-20°S.

Comparison of the eight sub-Figs of Fig.6 (Fig.6a-6h, respectively,) clearly show a similar pattern in the eastern part of the equatorial Atlantic. There are warm and cold SSTAs in this region, stretching further southwards along the coast of Central and South Africa. This is consistent with ACT development. There is no big spatial difference between a fully

developed strong and weak ACT. Comparing the patterns shown in Fig.6 with that of the first EOF presented in Fig.2a, we observe that individual PCA modes represent only a single spatial pattern of the first mode of NLPCA with standing oscillations. Fig.6a is similar to Fig.2a, hence NLPCA mode 1 includes PCA mode 1. The strong and weak ACT states, (Fig.6.a), (Fig.6h), respectively, are confined to the eastern part of the equatorial Atlantic. One of these patterns can be captured by a conventional PCA analysis but does not capture the quasi symmetry presented by *strong* and *weak* ACTs. The spatial distribution is best described (Fig.6) by NLPCA than PCA, and the variance may be represented by these first NLPCA modes. The asymmetry of SSTA in the evolution of NLPCA mode 1 is modest; the canonical and non canonical Atlantic El Niño event is observed which cannot be pointed out by linear mode 1.

It is not necessary to study RPCA since neither the PCA nor RPCA can represent the two states of ACT simultaneously. In contrast, the first NLPCA mode successfully passes through the strong and weak states as NLPC varies continuously from its minimum to maximum value. Therefore the rotated eigenvectors does not improve much on the unrotated eigenvectors for the study of ACT and Atlantic Niño.

The quasi-symmetry determined by a composite analysis (Fig.7) shows just two steps of ACT. These two maps correspond to the SSTA patterns of an average warm and cold ACT event, respectively. Since composite analysis is based on composite means, there will be difference of the micro-spatial patterns of strong and weak ACT from that of the NLPCA analysis. The very weak spatial asymmetry between cold and warm events of ACT observed in NLPCA mode 1 is manifest in composite analysis. These two maps correspond to the SSTA patterns of an average *weak* and *strong* ACT, respectively. Fig.7a and Fig.7b, respectively, bears a strong resemblance to Fig.6h and Fig.6a; and are strongly similar to EOF1. This means that EOF1 exhibits strong ACT. It is more explicit in the first NLPCA mode 1, which shows both strong and weak ACTs. Note that, consistent with the maps corresponding to the 1D NLPCA approximation (Fig.6h), the largest SSTA tend to be located in the Angola coast during the average strong and weak ACT events. The spatial correlation between the two maps is −0.99. This confirms the quasi-symmetry between the warm and cold ACT events.

Composite analysis can show only the states of the means of the weak and strong ACTs separately. But NLPCA shows different states of ACT; isolating different patterns and their associated amplitudes which may be missed by the means or averaging. The NLPCA, therefore, has the nice feature of capturing a range of variability between the symmetry of different ACT states, something that is difficult to obtain using index-based SST composites.

NLPCA improves on PCA by allowing low-dimensional approximations to have a structure other than that of simple standing oscillations. Both the NLPCA mode 1 and the composite analysis describe the symmetry between averages of warm and cold ACT events. However, NLPCA has the advantage of no a priori specification of a time series (e.g. periods) over which to composite, and provides a full 1D approximation to the data, in contrast to the absence of approximation in composite analysis. The latter can only give the mean state of ACT but PCA and NLPCA can approximate the real state. The fact that we observed that ACT is almost linear gives the impression that NLPCA is not necessary, but the implementation of only linear PCA hides this weak nonlinearity. The warm events (Atlantic Niños) are associated with reduced cold tongue development (Carton and Huang, 1994).

A final comparison of the 1D NLPCA and 1D PCA approximations is given in Fig.11, which shows, respectively, maps of the pointwise correlation between the original SSTA data and the 1D PCA approximation, and of the pointwise correlation between SSTA and the 1D NLPCA approximation (Fig.11). The two approximations are equally well correlated with the original data over the central band of the Atlantic Ocean, where the NLPCA correlations are somewhat higher than those of the PCA approximation, except in the Nothwest part of the Ocean. In the East region and in the ACT area the 1D NLPCA approximation displays a greater fidelity to the original data, as determined by the pointwise correlation, than does the 1D PCA approximation. This demonstrates the better capacity of NLPCA in representing SST data than the PCA. We observe that NLPCA represents better ACT surface on the Angolan coast than the PCA. However strong correlation in Fig.11 centered in the Nothwest part of the Ocean at around 20°W shows the ability of PCA to reproduce SSTA data in this region. Therefore, the NLPCA and PCA are complementary. These two statistical tools do not strongly represent globally SSTA data very close along the Guinea coast. As already mentioned above, in terms of explained variance, NLPCA mode 1 is generally greater than PCA mode 1 however the difference is not as much as that between PCA mode 2 and NLPCA mode 2, which are very large and with the NLPCA mode 2 being greater than PC mode 2.

The meridional mode (Figs.9) is more nonlinear than that of the ACT (Figs.6). We observe that the asymmetry of the variability of the meridional mode is more prononced (Fig.9a) than that of the ACT.

It was pointed out by Houghton and Tourre (1992) and confirmed by Metha (1998) that the northern and southern hemispheres appear to act independently. Regarding the Southern lobe picture of Figs.8 compared to other analysis we see that NLPCA gives the additional

information that this lobe underwent an eastward displacement. Also the weak gradient between the two lobes is observed in the sequence map; this weakening of the meridional mode is consistent with previous works (Tokinaga et al., 2011). This means that the second NLPCA mode has fully captured the Atlantic dipole pattern, unlike PCA mode 2, which only captured part. Thereby yielding a more accurate description of the Atlantic dipole (Fig.8) than the second PCA mode (Fig.2b), which did not fully represent the displacement of the center of action located in the southern part. With a linear approach, it is generally impossible to have simultaneous results. And also what is quite interesting is that previous statistical and diagnostic studies seem not to be interested in the investigation of the stability of spatial variability of the Atlantic dipole structure.

The weakness of the gradient between the North-West and south-West means that the Atlantic dipole is insignificant during some years. This result is supported by Tokinaga et al. (2011); they showed that CMIP3 twentieth century experiments tend to feature a weakening meridional SST gradient. Fig.9 confirms the nonlinearity observed in the characteristic of spatial variability of the meridional mode.

5. Conclusion

We have investigated the application of linear PCA and nonlinear generalization of PCA, to tropical Atlantic SST. It was observed that a NLPCA mode 1 explains 38% of the total variance in the SST field, in contrast to 36% for the first PCA mode while NLPCA SST mode 2 explains 22% of the total data variance compared to 16% by the linear PCA mode 2. PCA mode 1 also characterizes average ACT variability, but only as a standing oscillation, so it is unable to evaluate the weak asymmetry in spatial pattern between average warm and cold events manifested in the 1D NLPCA. Compared to PCA, NLPCA can better point out the ACT, Atlantic dipole, Canonical and non-canonical Atlantic Niño. NLPCA can better represent all the SST data than PCA. The Atlantic equatorial mode which is similar to El Niño/Southern Oscillation (ENSO) in the Pacific Ocean has been recognized and considering the Hsieh (2004) work, it is observed that it is less linear than the latter. The non linearity in spatial variation of ACT is modest in the Atlantic Ocean in contrast to the Pacific Ocean.

The NLPC mode 2 described the Atlantic dipole variability. The explained variance results show that the NLPCA mode 2 explains more variance as the second principal components. The first two NLPCA modes between them explain marginally more of the total data variance than do the first two PCA modes. We observed that the Atlantic dipole is more asymmetric

than Atlantic Niño. We have shown that the NLPCA serve as a useful tool to investigate various aspects of the Atlantic phenomena. For example, differences between the weak and strong ACTs, between the Atlantic canonical and non-canonical Atlantic Niño, and some of different states.

Overall, the mechanisms controlling the mean state of the tropical Atlantic are not fully understood. However, its mean state is important as an indicator for predicting future atmospheric circulation. Future analysis is needed to further explore the West African monsoon rainfall using NLPCA and the intended implications of SST for the spatio-temporal variability of precipitation over West Africa.

Acknowledgements This work was supported by the Mwalimu Nyerere African Union Scholarship Scheme (MNAUSS). The authors would like to thank Prof. Hsieh W. William for his guidance and suggestion on an early draft of the paper.

References

Carton, J. A., and Huang B.: Warm events in the tropical Atlantic, J. Phys. Oceanogr., 24, 888- 903, 1994. Doi:10.1175/1520-0485(1994)024%3C0888:weitta%3E2.0.co;2

Chen, H., Yin, B., Fang, G. and Wang, Y.: Comparison of nonlinear and linear PCA on surface wind, surface height, and SST in the South China Sea, Chin. J. Oceanol. Limnol., 28, 981-989, 2010. Doi:10.1007/s00343-010-9074-6

Clara, D., Michael, Alexander, A., Xie, S.-P., Adam, S.P.: Sea Surface Temperature Variability: Patterns and Mechanisms, Annu. Rev. Mar. Sci. 2, 115-143, 2010. Doi:10.1146/annurev-marine-120408-151453.

Czaja, A., Vaart, P. V. D.,Marshall, J.: A diagnostic study of the role of remote forcing in tropical Atlantic variability, J. Climate, 15, 3280-3290, 2002. Doi: 10.1175/1520-0442(2002)015%3C3280:adsotr%3E2.0.co;2

Delecluse, P., Servain, J., Levy, C., Arpe, K., Bengtsson, L. : On the connection between the 1984 Atlantic warm event and the 1982-1983 ENSO, Tellus, 46A, 448-464, 1994. Doi: 10.1034/j.1600-0870.1994.t01-1-00009.x

Delecluse, P., Servain, J., Levy, C., Arpe, K., Bengtsson, L. : Tropical Atlantic SST variability and its relation to El Niño Southern Oscillation, J. Geophys Res., 102, 929-945, 1997. Doi:10.1029/96jc03296.

Caniaux, G., Giordani, H., Redelsperger, J.-L., Guichard, F., Key, E., and Wade, M.: Coupling between the Atlantic cold tongue and the West African monsoon in boreal spring and summer, J. Geophys. Res., 116, C04003, 2011. Doi:10.1029/2010jc006570

Handoh, I., C., and Bigg, G., R.: A self-sustaining climate mode in the tropical Atlantic, 1995-1997: Observations and modelling, Quart. J. Roy. Meteor. Soc., 126, 807-821, 2000. Doi: 10.1002/qj.49712656403.

Hagos, S.M., and Cook, K.H.: Development of a coupled regional model and its application to the study of interactions between the West African monsoon and the eastern tropical Atlantic ocean, J. Climate, 22, 2591-2604, 2009. Doi:10.1175/2008jcli2466.1.

Hastenrath, S., Lamb, P.J.: Climatic Atlas of the Tropical Atlantic and Eastern Pacific Ocean, the University of Wisconsin Press, Madison, 15, 97 charts, 1977.

Hirst, A. C., and Hastenrath, S.: Atmosphere-ocean mechanisms of climate anomalies in the Angola tropical Atlantic sector, J. Phys. Oceanogr., 13, 1146-1157, 1983. doi: 10.1175/1520-0485(1983)013%3C1146:aomoca%3E2.0.co;2

Houghton, R.W.: Seasonal variations of the subsurface thermal structure in the Gulf of Guinea, Journal of Physical Oceanography, 13, 2070-2081, 1983. Doi:10.1175/1520-0485(1983)013%3C2070:svotst%3E2.0.co;2

Horel, J. D., Kousky, V. E., Kagaro, M. T.: Atmospheric conditions in the tropical Atlantic during 1983 and 1984, Nature, 322, 243-245, 1986. Doi:10.1038/322248a0

Huang, B., Schopf, P.S., Pan, Z.: The ENSO effect on the tropical Atlantic variability: A regionally coupled model study, Geophys. Res. Lett., 29(21), 2039, doi: 10.1029/2002GL 014872, 2002.

Huang, B., and Shukla, J.: Characteristics of the interannual and decadal variability in a general circulation model of the tropical Atlantic Ocean, J. Phys. Oceanogr., 27, 1693-1712, 1997. Doi: 10.1175/1520-0485(1997)027%3C1693:cotiad%3E2.0.co;2

Hsieh, W.W.: Nonlinear principal component analysis by neural networks, Tellus, 53, 599-615, 2001. Doi: 10.1034/j.1600-0870.2001.00251.x

Hsieh, W. W.: nonlinear multivariate and time series analysis by neural network methods, Review of Geophysics, 42, RG1003, 1-25, 2004. Doi: 10.1029/2002rg000112

Hsieh, W.W.: Nonlinear principal component analysis of noisy data. Neural Networks, 20, 434-443, 2007. Doi: 10.1016/j.neunet.2007.04.018

Fukuoka, A.: A Study of 10-day Forecast (A Synthetic Report), the Geophysical Magazine: Tokyo, 12, 177-218, 1951.

Lorenz, E.N.: Empirical Orthogonal Functions and Statistical Weather Prediction,Technical report, Statistical Forecast Project Report 1, Dep of Meteor, MIT: 49, 1956.

Hannachi, A., Jolliffe, I. T. and Stephenson, D. B.: Empirical orthogonal functions and related techniques in atmospheric science: A review. , International Journal of Climatology, 27, 1119-1152, 2007. Doi: 10.1002/joc.1499

Jackson, J.E.: A Users Guide to Principal Components. Psychometrika, New York: Wiley, 1991. Doi: 10.1002/0471725331

Joke F. Lübbecke and Michael J. McPhaden: A Comparative Stability Analysis of Atlantic and Pacific Niño Modes. J. Climate, 26, 5965-5980, 2013. Doi: 10.1175/jcli-d-12-00758.1

Kaiser, H. F.: The Varimax Criterion for Analytic Rotation in Factor Analysis. Psychometrika, 23, 187-200, 1958. Doi: 10.1007/bf02289233

Katz, E. J.: Waves along the equator in the Atlantic. J. Phys. Oceanogr., 27, 2536-2544, 1997. Doi: 10.1175/1520-0485(1997)027%3C2536:wateit%3E2.0.co;2

Kramer, M. A.: Non-linear principal component analysis using auto associative neural networks, AIChE J., 37, 233-243, 1991. Doi: 10.1002/aic.690370209

Von Storch, H., and Zwiers, F. W.: Statistical Analysis in Climate Research, Cambridge Univ. Press, New York, 484 pp, 1999. Doi: 10.1017/cbo9780511612336

Landman, W. A., and Tennant, W. J.: Statistical downscaling of monthly forecasts, Int. J. Climatol.,20,1521-1532.,2000.Doi: 10.1002/1097 0088(20001115)20:13%3C1521::aid-joc558%3E3.0.co; 2-n

Leonard, M. D., and Matthew, F.: The impact of the Atlantic cold tongue on West African monsoon onset in regional model simulations for 1998-2002, Int. J.Climatol.,35,275-287 2014. Doi: 10.1002/joc.3980

Latif, M., and Grötzner, A.: The equatorial Atlantic oscillation and its response to ENSO. Climate Dyn., 16, 213-218, 2000. Doi: 10.1007/s003820050014

Li, S., Hsieh W.W. and Wu A.:Hybrid coupled modeling of the tropical Pacific using neural networks, J. Geophys. Res., 110, 2005. Doi: 10.1029/2004JC002595

Li, T., and Philander, S.G.H.: On the seasonal cycle of the equatorial Atlantic Ocean, J. Climate, 10, 813-817, 1997. Doi: 10.1175/1520-0442(1997)010%3C0813:otscot%3E2.0.co;2

Merle, J., Fieux, M. and Hisard, P.: Annual signal and interannual anomalies of sea surface temperature in the eastern equatorial Atlantic Ocean, Deep Sea Res., 26, 77-101, 1980. Doi: 10.1016/b978-1-4832-8366-1.50023-6

Monahan, A. H.: Nonlinear principal component analysis: Tropical IndoPacific sea surface temperature and sea level pressure, J. Clim., 14, 219-233, 2001. Doi: 10.1175/1520-0442(2001)013%3C0219:npcati%3E2.0.co;2

Metha, V. M.: Variability of the tropical ocean surface temperatures at decadal-multidecadal time scales. Part I: The Atlantic Ocean, J. Clim., 11, 2351-2375, 1998. Doi: 10.1175/1520-0442(1998)011%3C2351:vottos%3E2.0.co;2

Moore, D. W., Hisard, P., McCreary, J. P., Merle, J., OBrien, J. J., Picaut, J., Verstrate, J.-M., Wunsch, C.: Equatorial adjustment in the eastern Atlantic., Geophys. Res. Lett., 5, 637-640, 1978. Doi: 10.1029/gl005i008p00637

Odekunle, T. O., and Eludoyin, A. O.: Sea surface temperature patterns in the Gulf of Guinea: their implications for the spatio-temporal variability of precipitation in West Africa, Int. J. Climatol. 28, 1507-1517, 2008. Doi: 10.1002/joc.1656

North, G. R., T. L. Bell, R. F. Cahalan, and F. J. Moeng: Sampling errors in the estimation of empirical orthogonal functions, Mon. Weather Rev., 110, 699-706, 1982. Doi: 10.1175/1520-0493(1982)110%3C0699:seiteo%3E2.0.co;2

Okumura, Y., and Xie, S.P.: Interaction of the Atlantic equatorial Cold Tongue and the African Monsoon, J. Climate, 17, 3589-3602, 2004. Doi: 10.1175/1520-0442(2004)017%3C3589:iotaec%3E2.0.co;2

Picaut, J: Propagation of the seasonal upwelling in the eastern equatorial Atlantic, Geophys. Res. Lett., 13, 18-37, 1983. Doi: 10.1175/1520-0485(1983)013%3C0018:potsui%3E2.0.co;2

Picaut, J., Servain, J., Antonio, Busalacchi, J. and Seva, M.: Interannual Variability Versus Seasonal variability in the tropical Atlantic, Geophys. Res. Lett., 11, 8,787-790, 1984. Doi: 10.1029/gl011i008p00787

Reason, CJC and Rouault M.: Sea surface temperature variability in the tropical South Atlantic Ocean and West African rainfall. Geoph.Res. Lett. 33: L21705. DOI: 10.1029/2006/GL027145, 2006.

Rouault, M., Florenchie, P., Fauchereau, N., and C. Reason, J. C.: South east Atlantic warm events and southern African rainfall, Geophys.Res. Lett., 30(5), 8009, , 2003. doi:10.1029/2002GL014840.

Rajagopalane, B., Carton, J., A., and Nigam, S.: Observed decadal midlatitude and tropical Atlantic variability, Geophys. Res. Lett., 25, 3967-3970, 1998. Doi: 10.1029/1998gl900065

Ruiz-Barradas, Kushnir, Y., and Tourre, Y.: Structure of interannual-to- decadal climate variability in the tropical Atlantic sector, J. Climate, 13, 3285-3297, 2000. Doi: 10.1175/1520-0442(2000)013%3C3285:soitdc%3E2.0.co;2

Servain, J. : Simple climatic indices for the tropical Atlantic ocean and some applications., J. Geophys. Res., 96, 15137-15146, 1991. Doi: 10.1029/91jc01046

Servain, J., and Merle, J.: Interannual climate variations over the tropical Atlantic Ocean, NATO ASI Series, 16, Prediction of Interannual Climate Variations, edited by J. Shukla, Springer-Verlag, Berlin, 153- 171, 1993. Doi: 10.1007/978-3-642-76960-3_8

Servain, J., and Legler, D.M.: Empirical Orthogonal Function Analyses of Tropical Atlantic Sea Surface Temperature and Wind Stress: 1964-1979, Journal Of Geophysical Research, 91, 181- 191, 1986. Doi: 10.1029/jc091ic12p14181

Servain, J., Clauzet, G., and Wainer,I. C.: Modes of tropical Atlantic climate variability observed by PIRATA, Geophys. Res. Lett., 30, doi: 10.1029/2002GL01512, 2003.

Servain, J., I. Wainer, McCreary, J. P., and Dessier, A.: Relationship between the Equatorial and meridional modes of climatic variability in the tropical Atlantic. Geophys. Res. Lett., 26, 485-488, 1999. Doi: 10.1029/1999gl900014

Servain, J., Amault, S.: On forecasting abnormal climatic events in the tropical Atlantic Ocean. J. Phys. Ann. Geophysicae, 13, 995-1008, 1995. Doi: 10.1007/s00585-995-0995-x

Smith, T.M., Reynolds, R.W.:Extended Reconstruction of Global Sea Surface Temperatures Based on COADS Data (1854-1997), J. Climate, 16, 1495-1510, 2003. Doi: 10.1175/1520-0442-16.10.1495

Gámez, A. J., Zhou, C. S.,Timmermann A., and Kurths, J.: Nonlinear dimensionality reduction in climate data. Nonlinear Processes in Geophysics., 11, 393-398, 2004. Doi: 10.5194/npg-11-393-2004

Xie, S.-P. and Carton, J.A.: Tropical Atlantic Variability: Patterns, Mechanisms, and Impacts. Geophysical Monograph, AGU, Washington, D.C., 121-142, 2004. Doi: 10.1029/147gm07

Tang, Y., and Hsieh,W. W.: Nonlinear modes of decadal and interannual variability of the subsurface thermal structure in the Pacific Ocean, J. Geophys. Res., 108(C3), 3084, doi:10.1029/ 2001JC001236, 2003.

Tenenbaum, J. B. , de Silva, V. , and Langford, J. C.: A global geometric framework for nonlinear dimensionality reduction, Science, 290, 2319-2323, 2000. Doi: 10.1126/science.290.5500.2319

Wauthy, B.: Introduction a la climatologie du Golfe de Guinée. Océanogr. Trop., 18, 103-138, 1983.

Xie, S.-P. and Tanimoto, Y. : A pan-Atlantic decadal climate oscillation. Geophys. Res. 950 Lett., 25 ,2185-2188, 1998. Doi: 10.1029/98gl01525

Xie, S.-P., Tanimoto, Y., Noguchi, H., and Matsuno, T.: How and why climate variability differs between the tropical Atlantic and Pacific, Geophys. Res. Letters, 26, 1609- 1612, 1999. Doi: 10.1029/1999gl900308

Zebiak, S. E.: Air-sea interaction in the equatorial Atlantic region, J. Climate, 6, 1567-1586. 1993. Doi: 10.1175/1520-0442(1993)006%3C1567:aiitea%3E2.0.co;2

Roweis, S. T. and Saul, L. K.: Nonlinear dimensionality reduction by locally linear embedding, Science, 290, 2323-2326, 2000. Doi: 10.1126/science.290.5500.2323

Scholkopf, B., Smola, A., and Muller, K.-R.: Nonlinear component analysis as a kernel eigenvalue problem. Neural Computation,10, 1299-1319, 1998. Doi: 10.1162/089976698300017467

Thorncroft, C., Nguyen, H., Zhang, C., Peyrillé, P.: Annual cycle of the west African monsoon: regional circulations and associated water vapour transport. Q. J. R. Meteorol. Soc., 137, 129-147, 2011. Doi: 10.1002/qj.728

Tokinaga.H. and Xie S.P.: weakening of the equatorial Atlantic cold tongue over the past six decades. Nature Geoscience. 4. 222-226. 2011. Doi: 10.1038/ngeo1078

Hastie, T. and Stuetzle, W.: Principal curves. Journal of the American Statistical Association, 84:502-516, 1989. Doi: 10.1080/01621459.1989.10478797

Aho, A. V., Hopcroft, J. E., and Ullman, J. D.: Data Structures and Algorithms. Addison-Wesley, June 1983. Doi: 10.1002/bimj.4710260406

Bachmann, C. M., Ainsworth, T. L., and Fusina, R. A.: Improved manifold coordinate representations of large-scale hyperspectral scenes. IEEE T. Geosci. Remote, 44(10), 2786-2803, 2006. Doi: 10.1109/tgrs.2006.881801

De Silva V., and Tenenbaum, J. B.: Sparse multidimensional scaling using landmark points. Stanford Mathematics Technical Report, June 2004.

Hecht-Nielsen, R.: Replicator neural networks for universal optimal source coding. Science, 269, 1860-1863, 1995. Doi: 10.1126/science.269.5232.1860

Houghton, R. W., and Y. M. Tourre,: Characteristics of lowfrequency sea surface temperature fluctuations in the tropical Atlantic, J. Clim., 5, 765-771, 1992. Doi: 10.1175/1520-0442(1992)005%3C0765:colfss%3E2.0.co;2

Malthouse, E. C.: Limitations of nonlinear pca as performed with generic neural networks. IEEE Transactions on Neural Networks, 9, 165-173, 1998. Doi: 10.1109/72.655038

Monahan, A.H., Fyfe, J.C., and Pandolfo, L.: The vertical structure of winter time climate regimes of the northern hemisphere extratropical atmosphere, J. Climate, 16, 2005-2021, 2003. Doi: 10.1175/1520-0442(2003)016%3C2005:tvsowc%3E2.0.co;2

Richter, I., Behera, S.K.,Masumoto,Y.,Taguchi,B.,Sasaki,H., and Yamagata, T.: Multiple Causes of Interannual Sea Surface Temperature Variability in the Equatorial Atlantic Ocean, Nature Geosci,6, 43-47, 2012. Doi: 10.1038/ngeo1660

YUKO, O., and Shang-Ping,X.: Some Overlooked Features of Tropical Atlantic Climate Leading to a New Nio-Like Phenomenon, American Meteorological Society, 19, 5859-5879, 2006. Doi: 10.1175/jcli3928.1

Jouanno, J., Marin, F., Du Penhoat, Y., Molines, J. M., and Sheinbaum, J.:Seasonal modes of surface cooling in the gulf of guinea, Journal of Physical Oceanography, 41(7), 1408- 1416, 2011a. Doi: 10.1175/jpo-d-11-031.1

Jouanno, J., Marin, F., du Penhoat, Y., Sheinbaum, J., and Molines, J.-M.: Seasonal heat balance in the upper 100 m of the equatorial atlantic ocean. Journal of Geophysical Research: Oceans, 116, 1978-2012, 2011b. Doi: 10.1029/2010jc006912

Foltz, G. R., and M.J. McPhaden: Interaction between the Atlantic meridional and Niño modes, Geophys. Res. Lett., 37, L18604, 2010. Doi: 10.1029/2010gl044001

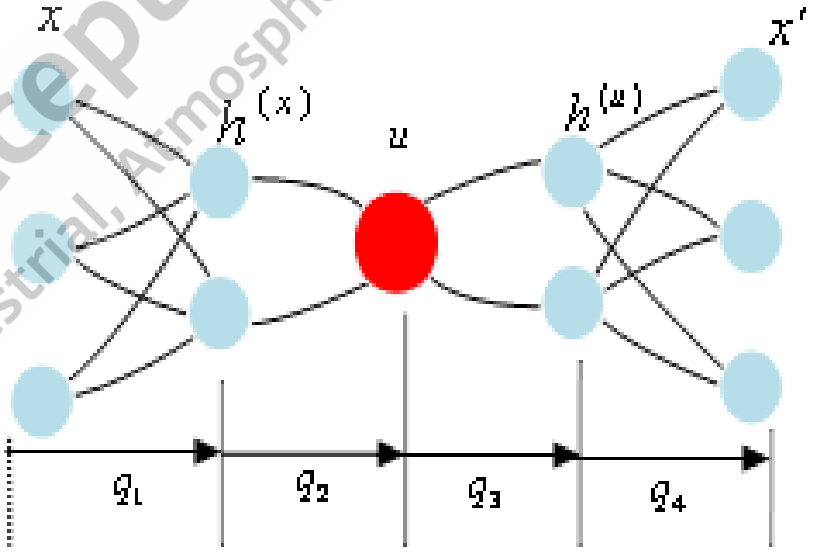

Fig. 1 The NN model for calculating nonlinear PCA. There are 3 'hidden' layers of variables or 'neurons' (denoted by circles) sandwiched between the input layer $\mathbf{x}$ on the left and the output layer $\mathbf{x}'$ on the right. Next to the input layer is the encoding layer, followed by

the 'bottleneck' layer (with a single neuron u for NLPCA), which is then followed by the decoding layer. q_1, q_2, q_3 and q_4 are the transfer functions.

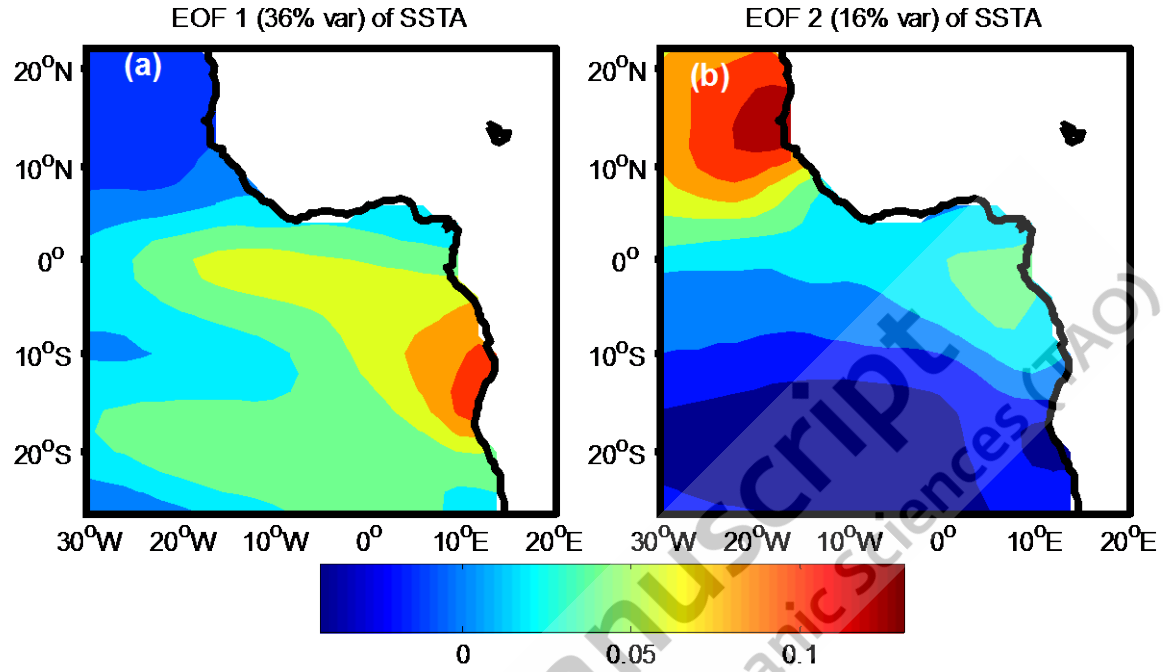

Fig. 2 Empirical orthogonal function (EOF) of detrended monthly sea surface temperature (SST) Anomalies. a) EOF1 mode (left) and b) EOF2 mode (right) with their explained variance in parenthesis. The contour interval is 0.01.

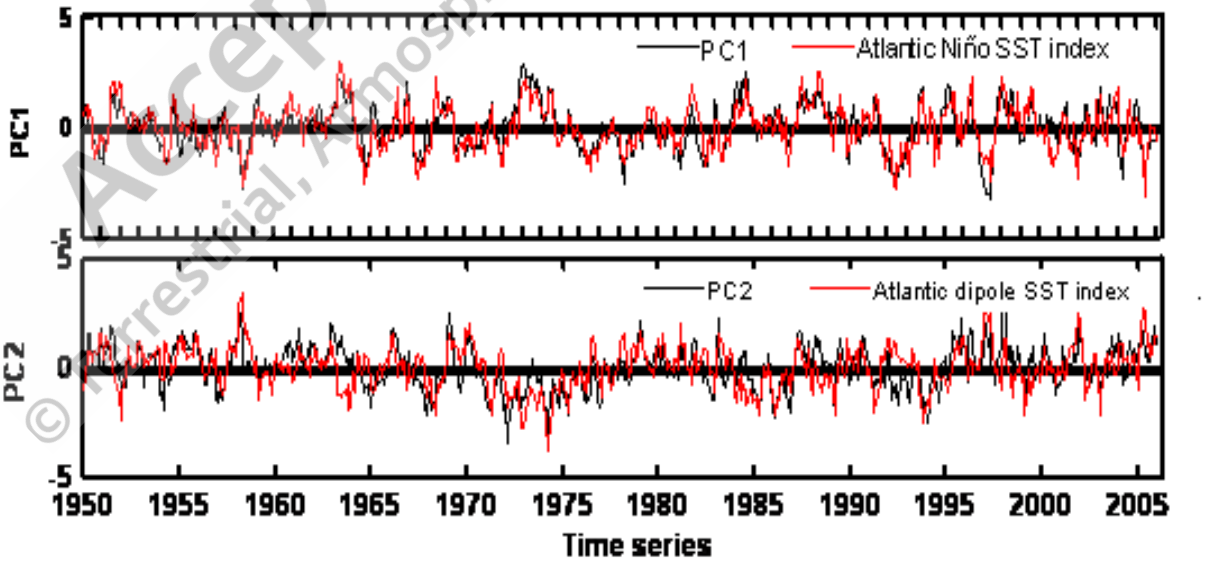

Fig. 3 The corresponding time coefficients in black, the Atlantic Niño index and Dipole index in red. Vertical lines in the time series correspond to January of the respective years, starting in January 1950 and ending in December 2005.

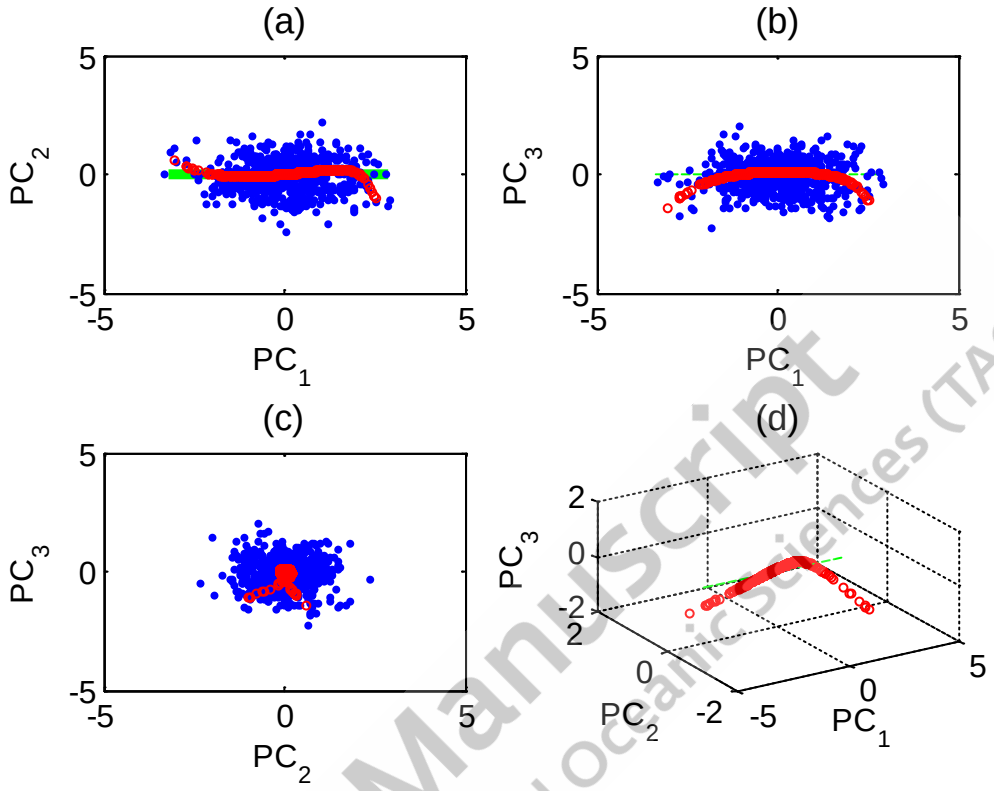

Fig. 4 Scatter plot of the sea surface temperature (SST) anomaly (SSTA) data (shown as blue dot) in the principal component (PC1, PC2, and PC3) plane. The first principal component analysis (PCA) eigenvector (green color) is oriented along the horizontal line. The first mode NLPCA approximation to the data is shown by the reds circles, which traced out a Wave-shaped curve.

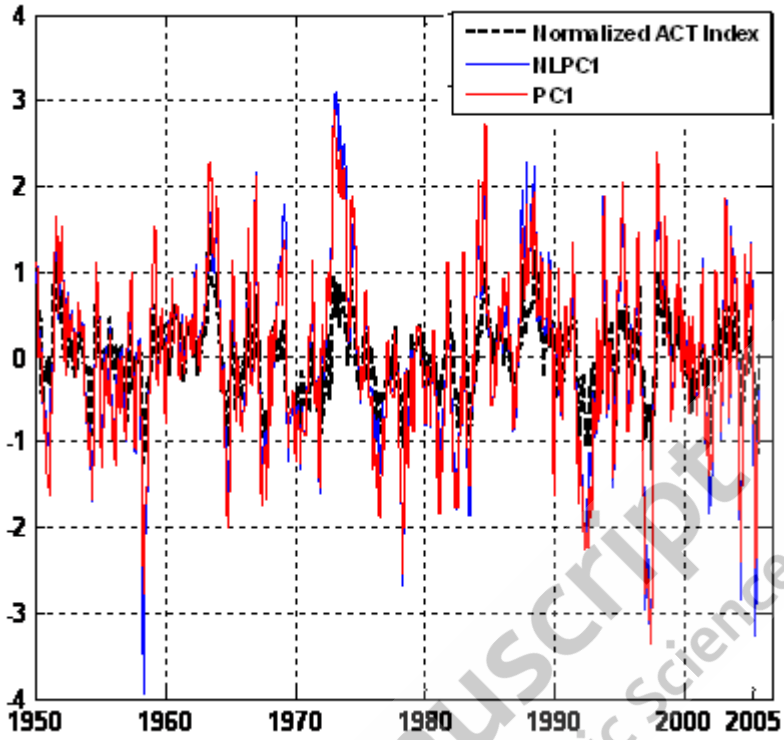

Fig. 5 Plot of NLPC1, the time series associated with SSTA NLPCA mode 1 (blue line), the normalized ACT index (black dashed line) and PC1 (red line).

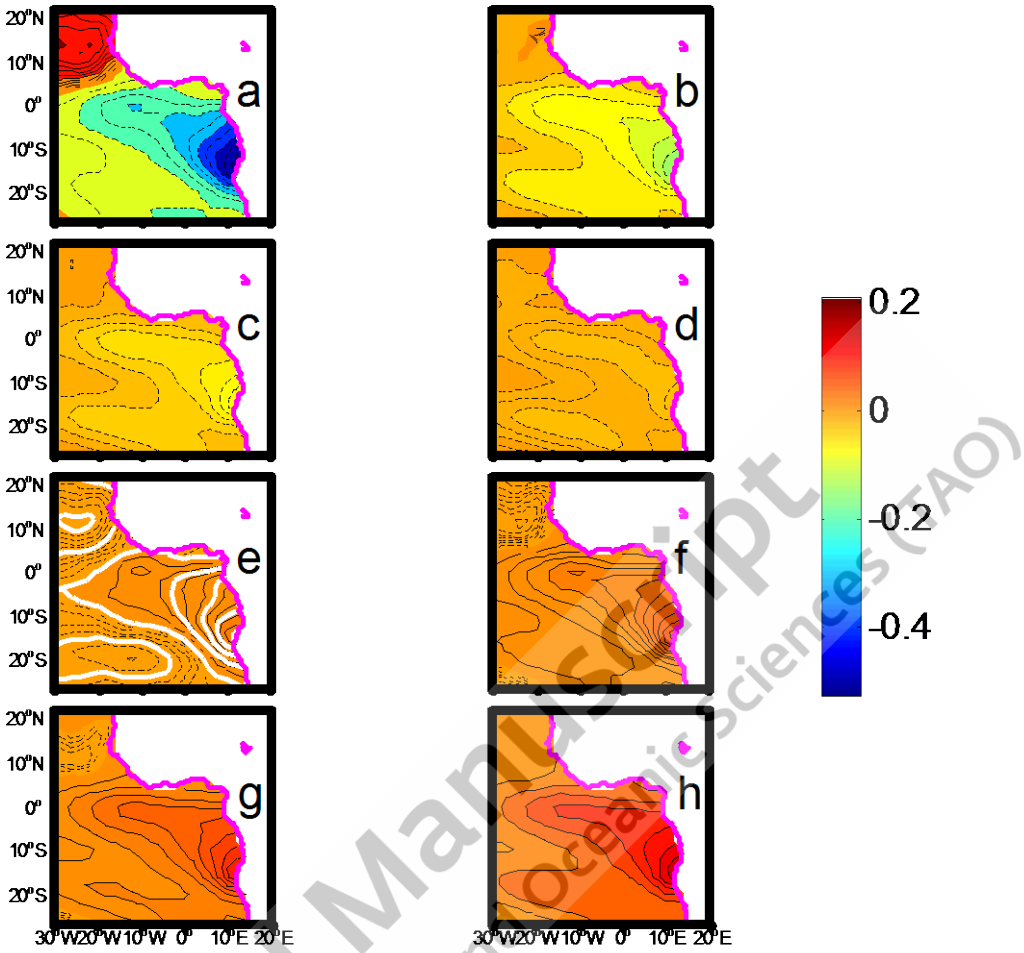

Fig. 6 The SST anomaly pattern (in °C) of the NLPCA as the minimum of NLPC **u** between June and August for each year of the first NLPCA mode. Considering just the eight minimum mentioned above, the anomaly pattern of the first NLPCA mode varies from (a) its minimum (strong Atlantic cold tongue), to (b) three-quarter its minimum, to (c) half its minimum, to (d) quarter of its minimum, to (e) quarter its maximum, to (f) half its maximum (non-canonical Atlantic Niño, to (g) three-quarter its maximum and (h) its maximum (weak Atlantic cold tongue). Zero contours are white lines. Positive contour is bold black line and negative contours are black. The contours in pink color are the coast.

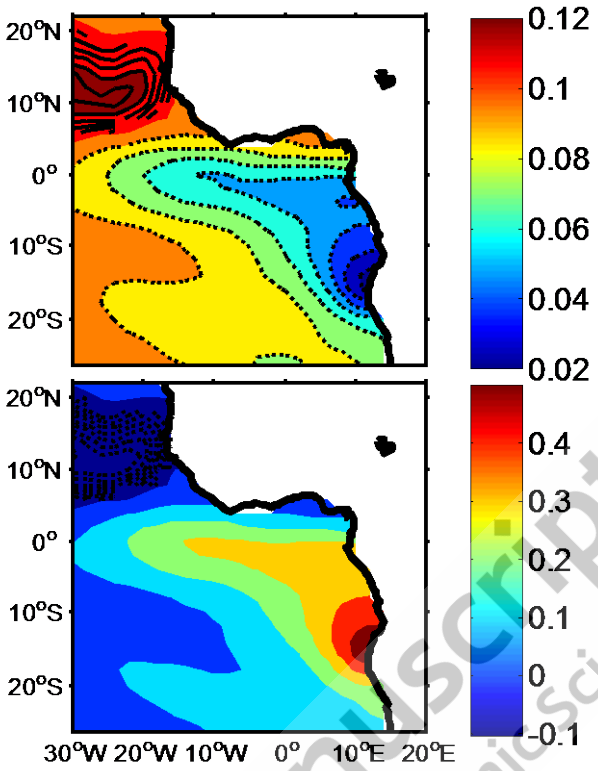

Fig. 7 Composite maps for average (a) cold ACT (upper) and (b) warm ACT (lower). Positive contours are black lines and negative contours are dashed black lines.

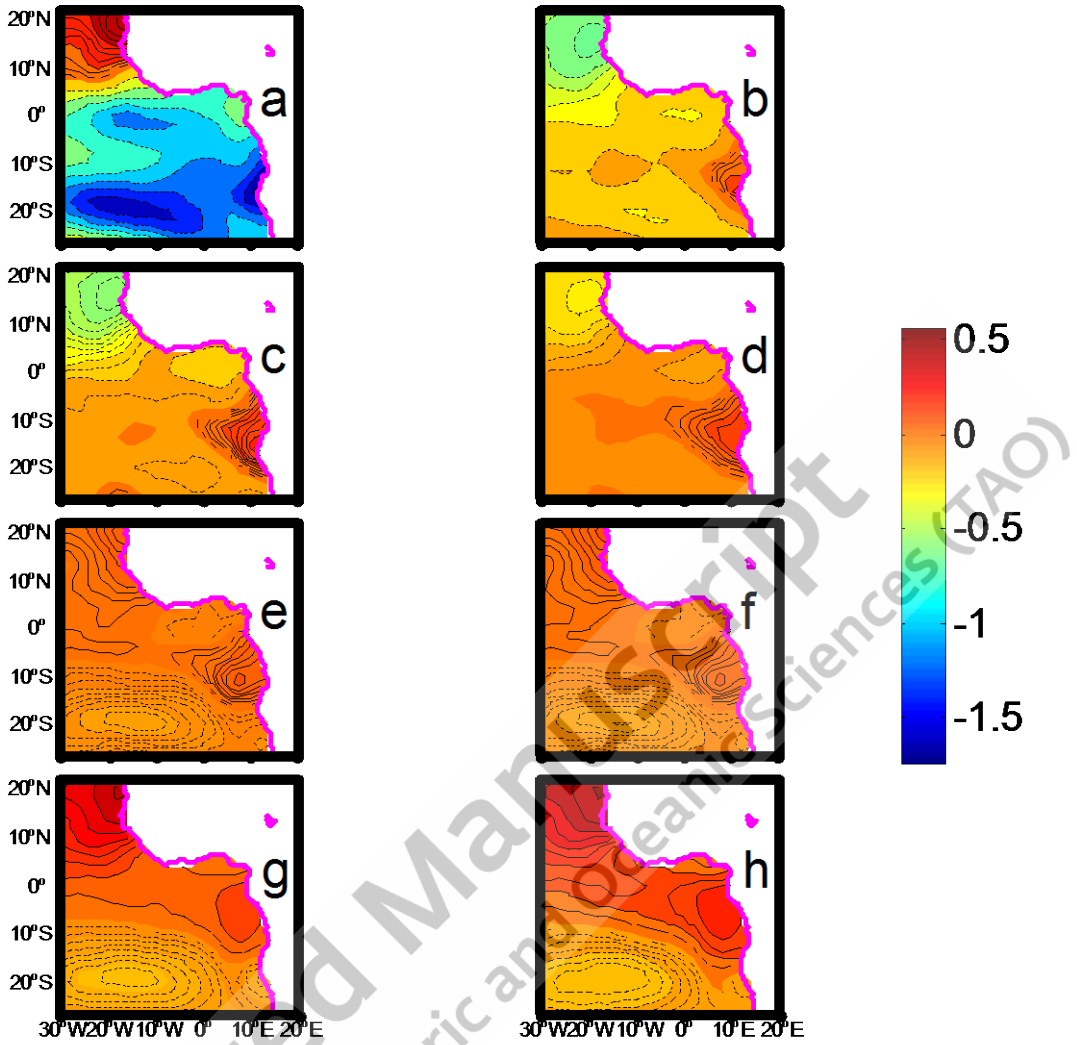

Fig. 8 The SST anomaly pattern (in °C) of the second NLPCA mode varies from (a) its minimum (*strong* gradient between north and South), to (b) three-quarter its minimum, to (c) half its minimum, to (d)quarter of its minimum, to (e) quarter its maximum, to (f) half its maximum, to (g) three-quarter its maximum and (h) its maximum (*weak* gradient between north and South). Zero contours are white lines. Positives contours are black line and negative contours are dashed black line. The contours in pink color are the coast.

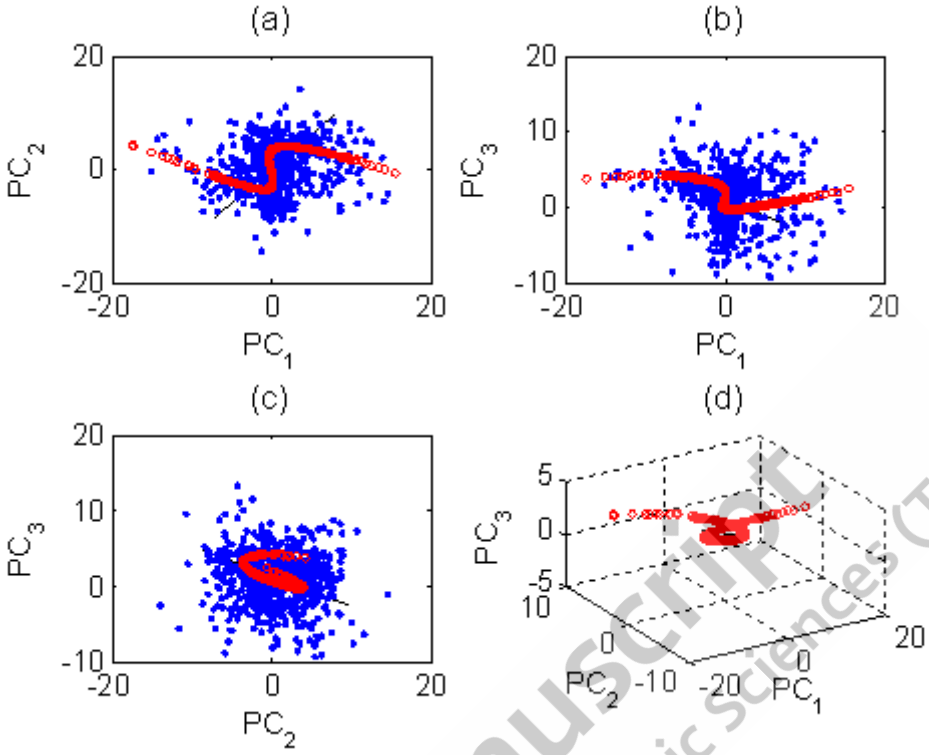

Fig. 9 Scatter plots of the sea surface temperature (SST) anomaly (SSTA) data (shown as blue dots) in the principal component (PC1, PC2, and PC3) plane. The dots show the residual data after the NLPCA mode 1 has been subtracted. This second mode NLPCA approximation to the data is shown by the reds circles, which trace out a Wave-shaped curve. (The linear solution to the dataset after NLPCA mode 1 has been removed is not the same as PCA mode 2, which is the linear solution to the dataset after PCA mode 1 has been removed.).

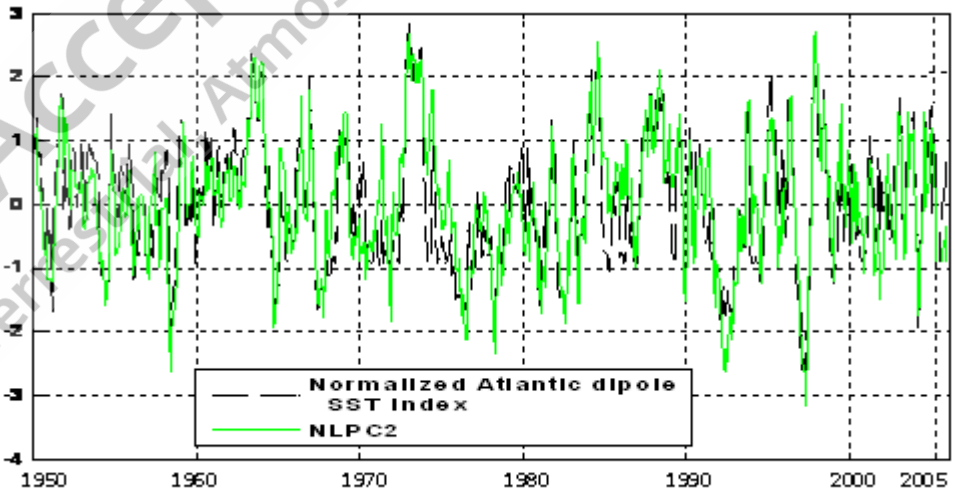

Fig. 10 Plot of NLPC2, the time series associated with SSTA NLPCA mode 2 (green line), the normalized Atlantic Dipole index (black dashed line).

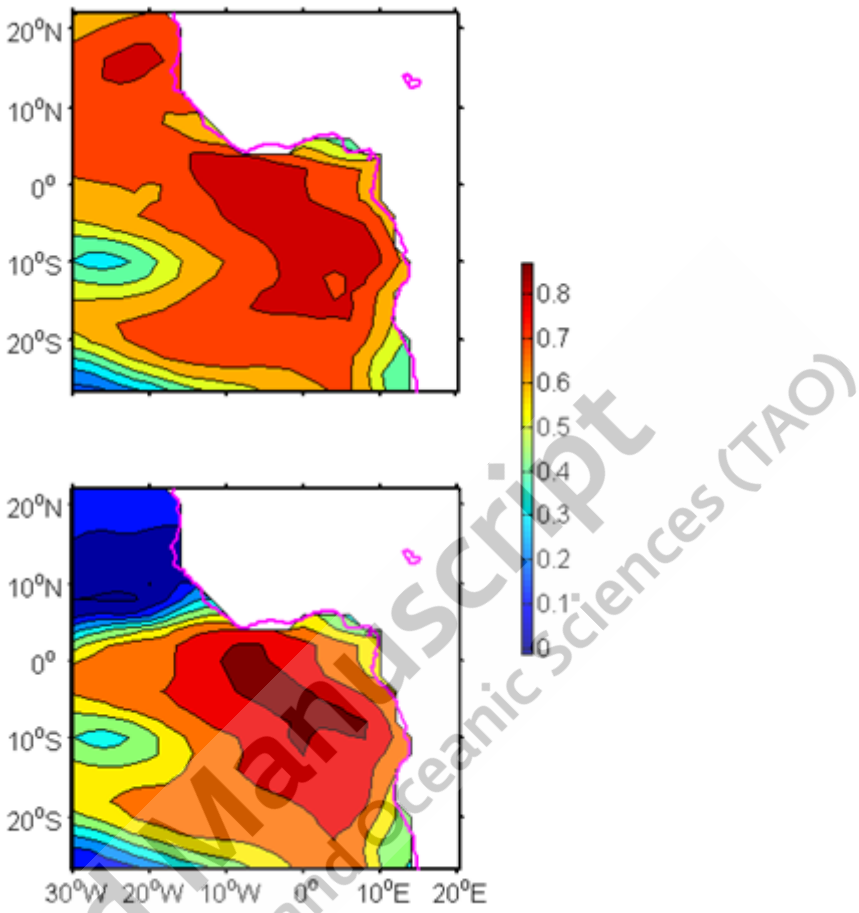

Fig. 11 Maps of pointwise correlation coefficients between observed SSTA (upper)and (a) 1D PCA approximation and (b) 1D NLPCA approximation (lower).